Available online at www.sciencedirect.com
SCIENCE DIRECT
Polymer 47 (2006) 1324–1332
polymer
www.elsevier.com/locate/polymer

Highly isotactic poly(vinyl alcohol) derived from *tert*-butyl vinyl ether. Part IV. Some physical properties, structure and hydrogen bonding of highly isotactic poly(vinyl alcohol) films

Hiroyuki Ohgi [a], Toshiaki Sato [a], Shaohua Hu [b], Fumitaka Horii [b,*]

[a] *Tsukuba Research Laboratories, Kuraray Co., Ltd, 41, Miyukigaoka, Tsukuba, Ibaraki 305-0841, Japan*
[b] *Institute for Chemical Research, Kyoto University, Uji, Kyoto 611-0011, Japan*

Received 20 August 2005; received in revised form 25 November 2005; accepted 11 December 2005
Available online 10 January 2006

Abstract

Some basic physical properties, structure and hydrogen bonding have been characterized for different stereoregular PVA films including highly isotactic PVAs (HI-PVAs), which were recently succeeded in synthesis, as functions of the *mm* fraction by using different analytical methods. The melting temperature, degree of crystallinity, and ^{13}C spin–lattice relaxation time of the crystalline component are found to have their own clear minima at the *mm* fraction of about 0.4–0.5. This fact suggests that structural disordering associated with the decrease in crystallinity may be most strongly induced at this *mm* fraction. The formation of the new crystal form of PVA has been reconfirmed for HI-PVAs with the *mm* fractions higher than about 0.55 by FTIR spectroscopy and the structure and hydrogen bonding have been investigated in detail by solid-state ^{13}C NMR spectroscopy. It is found that all OH groups are allowed to form successive intramolecular hydrogen bonding along the respective chains in the crystalline region for HI-PVAs with the *mm* fractions higher than about 0.7. Since these chains should contain some amount of *r* units even in the crystalline region, a slightly helical structure with a considerably long period may be adopted by them as an energetically stable state. On the basis of the line shape analysis of the CP/MAS ^{13}C NMR spectra of the crystalline components, structural causes of the appearance of the minima of the physical values described above are also discussed in relation to the introduction of disordered units mainly associated with hydrogen bonding to the syndiotactic or isotactic sequences forming successive intermolecular or intramolecular hydrogen bonding, respectively.

Keywords: Highly isotactic poly(vinyl alcohol); CP/MAS ^{13}C NMR; Hydrogen bonding

1. Introduction

A lot of investigations have been reported on the synthesis of stereoregular poly(vinyl alcohol)s (PVAs) which are rich in syndiotactic or isotactic sequences [1–3]. Marked stereoregularity dependencies on their physical properties were recognized, which may be mainly caused by differences in inter- and intramolecular hydrogen bonding. A series of vinyl esters have been polymerized using free radicals to prepare syndiotacticity-rich polymers and many studies have been reported on the relationships between stereoregularity and physical or solution properties of PVA [1–3]. On the other hand, the synthesis of isotactic PVA was carried out successfully using vinyl ethers, such as benzyl vinyl ether (BzVE) [4,5], *tert*-butyl vinyl ether (*t*BVE) [6,7], and trimethyl silyl vinyl ether (VOSi) [8,9] as starting monomers, and their physical or solution properties were also investigated [1–3].

Irrespective of many efforts paid to prepare stereoregular PVAs as described above, the stereoregularity still remained at a low level of $mm = 0.70$ even for so-called isotactic PVA (LI-PVA) derived from poly(trimethyl silyl vinyl ether) (PVOSi) [9,10]. Recently we studied in detail the cationic polymerization of *t*BVE with boron trifluoride diethyl etherate ($BF_3 \cdot OEt_2$) and successfully prepared the PVAs whose isotacticity is the highest of all isotacticity-rich PVAs reported so far [10–12]. We found that the reduction of $BF_3 \cdot OEt_2$ concentration to a level below 0.5×10^{-3} mol l^{-1} and the low mole ratio of $BF_3 \cdot OEt_2$/water of about 0.10 are essential factors to realize such high isotacticity. Preliminary experiments partly revealed interesting features of the highly isotactic PVA (HI-PVA) different from those of LI-PVA and ordinary atactic PVA (A-PVA) [10–13]. In this paper, some basic physical properties of PVA samples with different tacticities including HI-PVA are systematically examined by

* Corresponding author. Tel.: +81 774 38 3150; fax: +81 774 38 3148.
E-mail address: horii@scl.kyoto-u.ac.jp (F. Horii).

0032-3861/$ - see front matter © 2006 Elsevier Ltd. All rights reserved.
doi:10.1016/j.polymer.2005.12.036

different analytical methods as functions of the *mm* fraction at the wide range. Intramolecular and intermolecular hydrogen bondings are also characterized for HI-PVA in detail by using high-resolution solid-state ^{13}C NMR spectroscopy.

2. Experimental

2.1. Preparation of stereoregular PVAs

HI-PVAs with *mm* triad fractions higher than 0.70 were synthesized by the following procedure [11]: The *t*BVE monomer was prepared by the alkyl exchange reaction between *tert*-butyl alcohol and lauryl vinyl ether in the presence of $Hg(OAc)_2$. Solvents were purified and dehydrated carefully by the conventional methods. Toluene was distilled in the presence of metallic sodium before use. $BF_3 \cdot OEt_2$ was purified by distillation under reduced nitrogen pressure and used as a toluene solution. Polymerization of *t*BVE was carried out with $BF_3 \cdot OEt_2$ in toluene at −78 °C, and then the poly(*t*BVE) was converted into PVA by cleavage of the ether linkage using hydrogen bromide at 0 °C.

The previously reported LI-PVAs [11], which have *mm* triads lower than 0.70, were synthesized by the polymerization of *t*BVE with $BF_3 \cdot OEt_2$ in a mixture of toluene and methylene chloride at −78 °C and used as references to clarify unique solid properties of HI-PVAs. The *mm* fraction of LI-PVA decreases monotonically with increasing methylene chloride content. The commercially available A-PVA derived from poly(vinyl acetate) and syndiotacticitiy-rich PVA (S-PVA) derived from poly(vinyl pivalate) by using the method previously reported [14] were also used as reference samples.

2.2. Measurements of degrees of polymerization

In general, the viscosity-averaged degree of polymerization (P_v) of A-PVA is determined from its limiting viscosity number ([η]) measured in water at 30 °C [15]. However, since it was difficult to dissolve the stereoregular PVAs, especially HI-PVAs, in water, such samples were converted into poly(vinyl acetate) (PVAc) by acetylation. The P_v of PVAc was determined from [η] measured in acetone at 30.0 °C by using the following equation [16]:

$$[\eta] = 7.94 \times 10^{-4} \times P_v^{0.62} \quad (1)$$

2.3. Determination of stereoregularity of PVAs

The stereoregularity of PVA samples was determined on the basis of the methods [17,18] previously reported by solution-state ^1H NMR spectroscopy: ^1H NMR spectra were measured in deuterated dimethyl sufoxide (DMSO-d_6) at 25.0 °C on a JEOL GSX-270 spectrometer operating at 270.17 MHz.

2.4. Preparation of PVA films

All physical properties were measured on the PVA films with a thickness of about 100 μm unless otherwise specified. The PVA films were prepared by casting the 5 wt% DMSO solution on a glass plate, evaporating DMSO at 50 °C for 20 h, immersing them in hot methanol overnight, and then drying at 50 °C under vacuum.

2.5. Thermal analyses

Differential scanning calorimetry (DSC) thermograms were recorded on 10 mg of each PVA sample under nitrogen with a Mettler differential scanning calorimeter. Melting temperatures of the samples were determined as endothermic peak temperatures observed in the thermograms. An thermogravimetric analysis (TGA) was carried out on 10 mg of each sample under a nitrogen atmosphere. The heating rate was 10 °C/min in these measurements.

2.6. Fourier transform infrared spectroscopy

FTIR spectra of the stereoregular PVA films with about 25 μm in thickness were recorded on a Nicolet 520 FTIR spectrometer in the wave number range of 4000–500 cm^{-1}. Fast Fourier transforms were conducted after the accumulation of 32 scans.

2.7. Solid-state ^{13}C NMR spectroscopy

Cross polarization/magic angle spinning (CP/MAS) ^{13}C NMR spectroscopy was performed at room temperature on a JEOL JNM-FX200 spectrometer under a static magnetic field of 4.7 T. ^1H and ^{13}C radio-frequency field strengths $\gamma B_1/2\pi$ were 69 kHz in the CP process, whereas the ^1H field strength was reduced to 59 kHz for the dipolar decoupling. The CP contact time and MAS rate were set to 1 ms and 3.5 kHz, respectively. A MAS rotor with an O-ring seal [19,20] was employed not to allow each dried sample to adsorb atmospheric moisture during NMR measurements. The detailed procedure of the solid-state NMR measurements was almost the same as described in the previous papers [20–25].

3. Results and discussion

3.1. Characterization of stereoregular PVAs

The triad tacticities of HI-PVAs determined by solution-state ^1H NMR spectroscopy are listed in Table 1. For reference, the tacticities of LI-PVA derived from poly(*t*BVE), A-PVA derived from poly(vinyl acetate), and S-PVA derived from poly(vinyl pivalate) are also listed in this table. Here, these results can be evaluated in the same way as previously reported [26,27] on the basis of the simple stereoregular polymerization mechanism. When δ is defined as the persistence probability that an attacking monomer gives the same configuration (diad meso, *m*) as that of the last monomer residue, the following equations hold:

$$f_{mm} = \delta^2 \quad (2)$$

$$f_{mr} = 2\delta(1-\delta)$$

Table 1
The characterization of the stereoregular PVA samples

Sample	Tacticity in triad			Tacticity in diad		P_v[a]	T_m (°C)	ΔH (kJ mol^{-1})	T_d[b] (°C)
	mm	*mr*	*rr*	*m*	*r*				
HI-PVA1	0.791	0.189	0.020	0.886	0.114	3540	246.8	3.87	287
HI-PVA2	0.788	0.189	0.023	0.883	0.117	6800	248.8	3.79	280
HI-PVA3	0.781	0.189	0.030	0.876	0.124	23800	246.3	3.50	267
HI-PVA4	0.762	0.206	0.032	0.865	0.135	4800	243.8	2.89	260
LI-PVA1	0.634	0.295	0.071	0.782	0.218	9300	222.3	2.41	239
LI-PVA2	0.421	0.397	0.183	0.619	0.281	3450	212.0	–	186
A-PVA	0.220	0.050	0.280	0.470	0.530	1750	224.7	3.41	233
S-PVA	0.140	0.480	0.380	0.380	0.620	1700	247.1	4.31	247

[a] Viscosity-average degree of polymerization.
[b] 5 wt% loss temperature determined by TGA.

$$f_{rr} = (1-\delta)^2$$

where f_{mm}, f_{mr}, and f_{rr} are the mole fractions of the *mm*, *mr*, and *rr* sequences, respectively. The observed δ values were obtained from the f_{mm} values determined by solution-state ^{1}H NMR using Eq. (2) and the relationship between δ and the mole fraction (P) of each triad tacticity is shown in Fig. 1. Here, solid lines are the theoretical results calculated by Eq. (2).

As is clearly seen, the observed results are in good agreement with the theoretical ones for each triad tacticity in the wide range of δ including the higher values newly obtained in this work. This fact suggests that the growing chain end and its penultimate unit may admit the statistically random addition reaction of the monomer irrespective of the tacticity of the chain end. The diad tacticities calculated by using Eq. (2) are also listed in Table 1.

3.2. Thermal properties

As previously reported [10,11], HI-PVAs are further richer in isotacticity than the PVA samples derived from PVOSi [8,9] whose isotacticity was the highest of all isotactic PVAs so far.

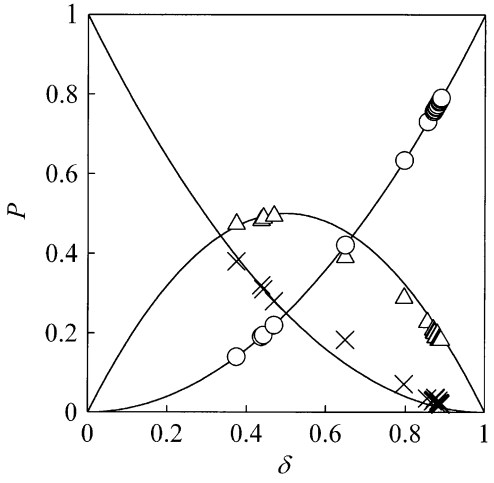

Fig. 1. Relationship between the fraction of meso diad (δ) and the probability (P) of the *mm* (circle), *mr* (triangle), or *rr* (cross) sequences for different stereoregular PVA samples. The solid curves indicate the theoretical values calculated by the Bovey's model [27].

We have first studied thermal behavior of HI-PVAs. Fig. 2 shows DSC thermograms measured for several stereoregular PVA samples at a heating rate of 10 °C/min. The melting temperature (T_m) determined as an endothermic peak top and the heat of melting (ΔH) estimated from the integrated intensity of the endothermic curve are also listed in Table 1 for each sample. The HI-PVA sample shows a rather sharper melting curve and a higher melting temperature similarly to the cases of S-PVA compared to A-PVA or LI-PVA. In contrast to the HI-PVA samples, it is difficult to determine the heat of melting (ΔH) for the LI-PVA samples because of its broad melting endothermic curve. This may be due to low heat stability of this sample, as shown later by TGA measurements. On the other hand, the glass–rubber transition cannot be clearly observed in each case in Fig. 2 but it should be noted here that the peak temperature of tan δ, which may correspond to the glass transition temperature estimated by dynamic viscoelastic measurements, was not significantly influenced by the difference in stereoregularity. The details of dynamic

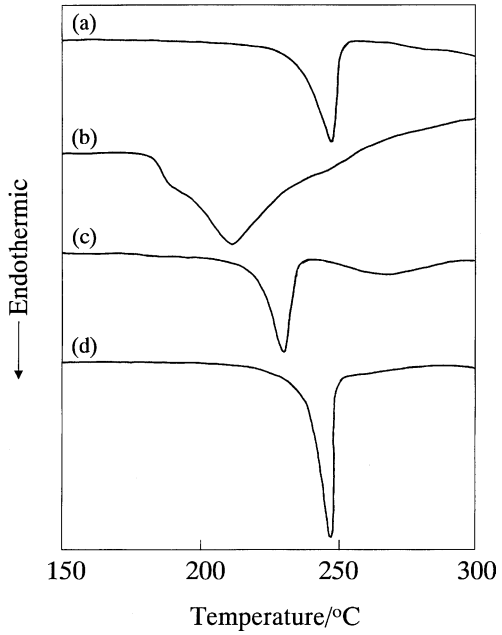

Fig. 2. DSC thermograms of different stereoregular PVA samples: (a) HI-PVA (*mm* = 0.78), (b) LI-PVA (*mm* = 0.42), (c) A-PVA, (d) S-PVA.

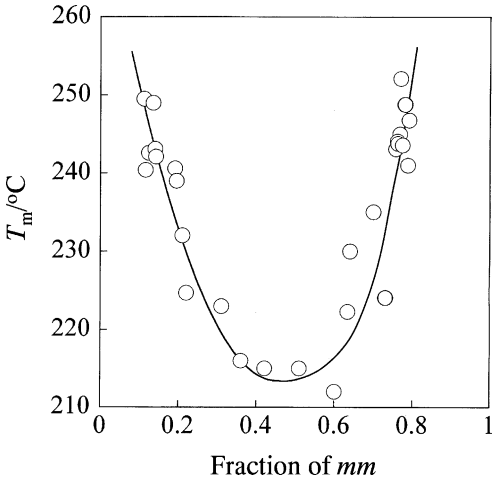

Fig. 3. Relationship between the *mm* fraction and the melting temperature (T_m) for different stereoregular PVA samples.

viscoelastic behavior of the stereoregular PVA samples will be reported elsewhere.

In Fig. 3 the T_m values determined by DSC are plotted against the *mm* fractions for the stereoregular PVAs. It is clearly found that the T_m greatly depends on the *mm* fraction and a marked minimum appears at $f_{mm} = \sim 0.50$. The cause of the appearance of the minimum at $f_{mm} = \sim 0.50$ will be discussed later after the detailed structural characterization is completed by solid-state ^{13}C NMR spectroscopy. Interestingly, the T_m of one of HI-PVAs is the highest of all PVA samples including S-PVAs. Here, A-PVAs show the T_m values ranging from 225 to 240°C as seen in Fig. 3. Such a somewhat wide distribution in T_m among these samples may be due to the differences in molecular weight or in a small amount of residual water.

A similar remarkable dependence on the *mm* fraction is also obtained from the observed enthalpy for the same stereoregular PVA samples, as shown in Fig. 4. It should be noted that a clear minimum appears also at the *mm* fraction of about 0.50 in this

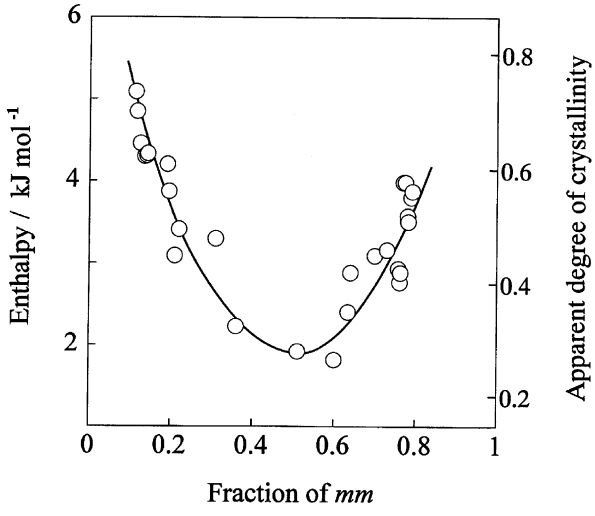

Fig. 4. Relationship between the *mm* fraction and the enthalpy ΔH for melting and the apparent degree of crystallinity estimated from ΔH for different stereoregular PVA samples.

case. In general, the degrees of crystallinity of A-PVA and S-PVA can be determined from the ΔH values obtained in the DSC measurements by assuming $\Delta H_c = 6.87$ kJ mol^{-1} for the 100% crystals [28] irrespective of the stereoregularity. However, the same ΔH_c value may not be used for the HI-PVA samples because the crystal structure of HI-PVA significantly differs from that of A-PVA or S-PVA [10]. Here, the apparent degrees of crystallinity were determined for HI-PVA by using the same ΔH_c because no determination of ΔH_c has not yet been made for these polymers. The apparent degrees of crystallinity thus obtained are shown against the right vertical axis in Fig. 4, for reference.

3.3. Thermal decomposition

TGA curves of the stereoregular PVA samples are shown in Fig. 5. As clearly seen in this figure, the first weight loss process for A-PVA (dotted line) occurs at 220–275 °C, followed by a further weight loss at 300–350 °C, leaving a residue of approximately 15 wt% at 400 °C. In contrast, the major weight loss of HI-PVA (bold line) takes place at 270–350 °C, leaving a residue of about 20 wt% at 400 °C. The 5 wt% loss temperature T_d, which is defined as the temperature where the 5% weight loss occurs, is also listed for each sample in Table 1. This table indicates that the order of the T_d is HI-PVA > S-PVA > A-PVA > LI-PVA. This order well corresponds to the order of T_m and thus HI-PVA has also the highest heat stability of all PVAs.

According to the previous studies of the thermal decomposition of A-PVA [29], the major pyrolysis product is water, which is produced by the elimination of the OH groups, and water begins to evolve at lower temperatures than the other degradation products such as aldehydes, ketones and benzene derivatives. Therefore, the initial weight loss should be due to the elimination of water for all PVA samples, and such elimination will preferably occur in the molten state of each PVA sample.

The second weight loss clearly observed for A-PVA and S-PVA in Fig. 5 should be due to other degradation products such as aldehydes and ketones. However, this process is not clear for HI-PVA and such different behavior may be due to

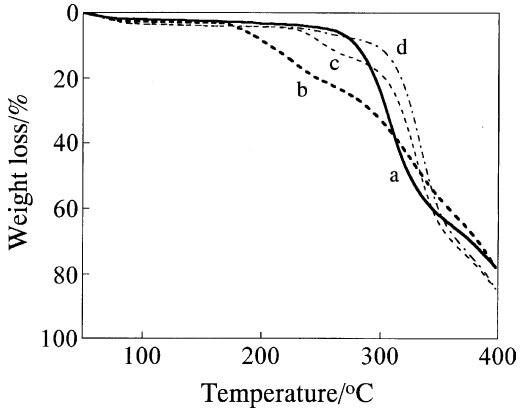

Fig. 5. TGA thermograms of different stereoregular PVA samples: (a) HI-PVA (*mm* = 0.78), (b) LI-PVA (*mm* = 0.42), (c) A-PVA, (d) S-PVA.

the difference in the chain-end structure in each polymer. More detailed experiments will be made in future including the characterization of the chain ends by considering the termination reaction during the polymerization.

3.4. FTIR spectra

Fig. 6 shows FTIR spectra of the stereoregular PVA samples. Remarkable intensity changes with the change in stereoregularity are observed for the 916 and 849 cm^{-1} bands, which are assigned to the CH_2 rocking motion or the skeletal motion and to the stretching of the C–C bond or the skeletal motion of the main chain, respectively [30]. The relationship between the absorbance ratio, D_{916}/D_{849}, of the two bands and the syndiotacticity expressed as $r\%$ was already proposed as follows [1,31]:

$$\text{syndiotacticity}(r\%) = (72.4 \pm 1.09)(D_{916}/D_{849})^{0.43+0.006} \quad (4)$$

In Fig. 7, the D_{916}/D_{849} ratios obtained for our present samples including HI-PVAs are plotted against the m and r fractions. As clearly seen in Fig. 7, the ratio continuously decreases with increasing r fraction in the whole region including the region for HI-PVA and the r fraction (f_r) is found to be well expressed

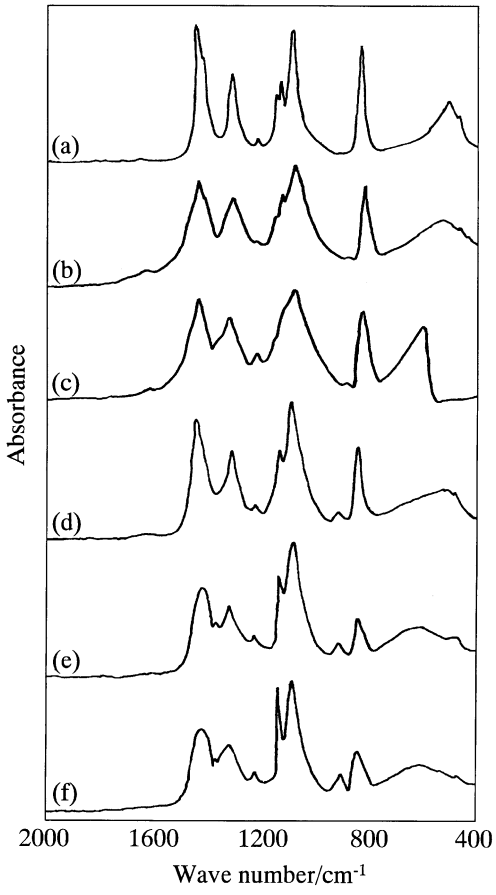

Fig. 6. FTIR spectra of different stereoregular PVA samples: (a) HI-PVA (mm=0.78), (b) HI-PVA (mm=0.67), (c) LI-PVA (mm=0.64), (d) LI-PVA (mm=0.42), (e) A-PVA, (f) S-PVA.

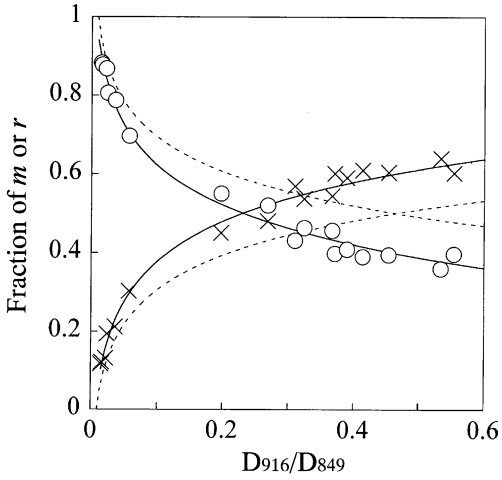

Fig. 7. Relationship between the fraction of the meso diad (circle) or the racemo diad (cross) and the D_{916}/D_{849} ratio for different stereoregular PVA samples. The broken and solid lines indicate the values calculated by using Eqs. (4) and (5), respectively.

by the following equation (solid line in the figure):

$$f_r = 0.713 + 0.334 \log(D_{916}/D_{849}) \quad (5)$$

For comparison, the corresponding relation derived from Eq. (4) is also depicted as a dotted line in Fig. 7. It is found that Eq. (4) does not hold in the present case. One of the causes for the discordance may be that the syndiotacticity ($r\%$) in Eq. (4) was determined by using the CH_3 proton resonance lines of PVAc in solution. Namely, the tacticity determination seems not to be carried out in a fully high precision because of the low resolution of the CH_3 resonance lines [1,32]. In contrast, the triad tacticity can be determined much more precisely by using the OH triplets [17] observed by ^1H NMR measurements of PVA in DMSO-d_6 and this method was used to obtain the f_r values shown in Fig. 7. Another remark is that the intensity of the 916 cm^{-1} band tends to be somewhat affected by the crystallization of PVA [1,33]. Since HI-PVAs have much higher degrees of crystallinity than the isotacticity-rich PVA samples used for the derivation of Eq. (4), some complicated effect of crystallinity may be included in the relationship between the f_r and D_{916}/D_{849} shown in Fig. 7.

Another remarkable spectral change in the stereoregular PVAs is observed for the band at 1140–1150 cm^{-1} in Fig. 6. This band is assigned to the C–C stretching vibration in the crystals, which is coupled with the C–O stretching, or to the O–C–C symmetric stretching vibration ascribed to the skeletal vibration of the atactic or syndiotactic part [30,32]. The intensity of the band was found to depend on the crystallinity [33] and, in accord with such previous finding, an intensity increase of the band is observed in S-PVA having higher crystallinity. Moreover, the band is hardly observed for the LI-PVA (mm=0.64) sample, probably because the crystallinity is very low in this sample as shown in Fig. 4.

In contrast, a new band appears at about 1165 cm^{-1} for HI-PVA and another band that may correspond to the original band is also observed at a slightly higher wave number in Fig. 6. This fact is due to the formation of another type of

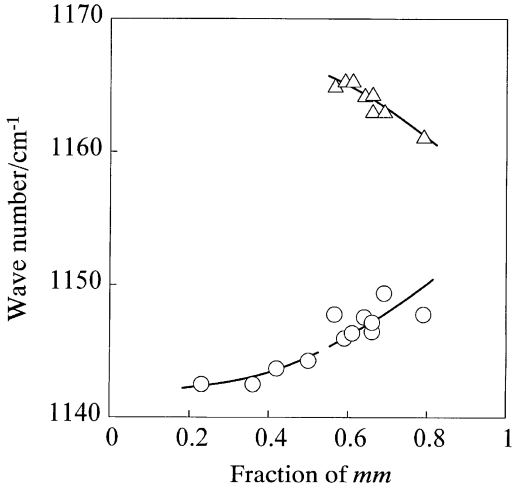

Fig. 8. Relationship between the *mm* fraction and the wave number of the crystalline band for different stereoregular PVA samples.

crystal form observed for HI-PVA [10–12]. Murahashi et al. also observed such two bands for their isotactic PVA derived from PVOSi but the intensities were very weak because of the low crystallinity [31]. In Fig. 8, the wave numbers of the crystalline bands appearing at 1140–1160 cm^{-1} are plotted against the *mm* fraction for all PVA samples used in this work. An evident boundary between the ordinary and new crystal forms is found to exist at the *mm* fraction of about 0.55. This value seems to agree with the value that gives the lowest crystallinity of PVA as shown in Fig. 4.

3.5. CP/MAS ^{13}C NMR characterization

Since the stereoregularity dependence of the physical properties of PVA may be closely related to inter- and intramolecular hydrogen bonding, it is very important to characterize such hydrogen bonding for the stereoregular PVAs in detail. As previously reported [34–40], CP/MAS ^{13}C NMR spectroscopy is very powerful in characterizing the structure of the crystalline and non-crystalline regions of semi-crystalline polymers. In the case of the crystalline component of solid A-PVA samples, the CH resonance line splits into a triplet due to the formation of 2, 1, and 0 intramolecular hydrogen bond(s) in the triad sequences having the all-*trans* conformation [20–25]. As for the non-crystalline component, the characterization becomes more complicated because of the effects of the *gauche* conformation and it may be successful when the statistical treatment will be allowable for the formation of intramolecular hydrogen bonding and for the generation of the *gauche* conformation [23–25]. Here, we apply the CP/MAS ^{13}C NMR analysis established for A-PVA [20–25] to the highly isotactic PVA samples.

Fig. 9 shows CP/MAS ^{13}C NMR spectra measured at room temperature for the PVA samples with different tacticities. As expected, the CH resonance lines basically split into three constituent lines in the respective samples and the relative intensities are greatly altered depending on the tacticity. To separate the contributions from the crystalline and

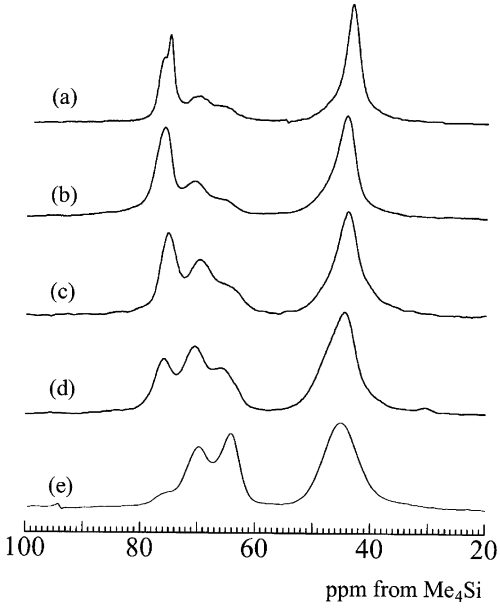

Fig. 9. CP/MAS ^{13}C NMR spectra measured at room temperature for different stereoregular PVA samples: (a) HI-PVA (*mm* = 0.79), (b) HI-PVA (*mm* = 0.70), (c) LI-PVA (*mm* = 0.59), (d) LI-PVA (*mm* = 0.50), (e) A-PVA.

non-crystalline regions, ^{13}C spin–lattice relaxation behavior was measured at room temperature for each sample by the CPT1 pulse sequence as reported previously [20–22,24,25]. In accord with the results of the different A-PVA samples [20–22,24,25], it was also found that there exist two components with different T_{1C} values for each sample. Since longer T_{1C} implies less molecular mobility for solid PVA under the present experimental condition, the components having a longer and shorter T_{1C} should be assigned to the crystalline and non-crystalline components, respectively, as the cases of A-PVA [20–22,24,25].

Fig. 10 shows a plot of the T_{1C} values of the crystalline components thus obtained for the CH lines as a function of the *mm* fraction. In good accord with the cases of T_m and

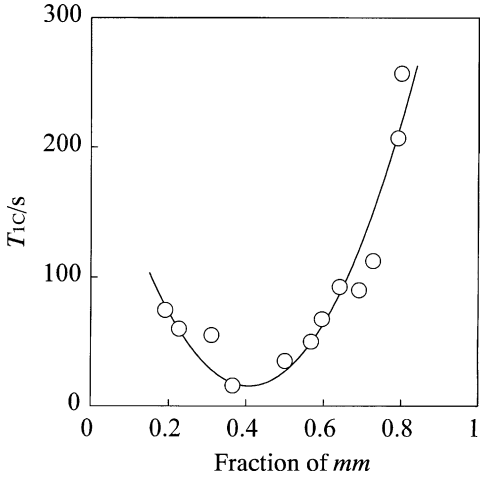

Fig. 10. Relationship between the fraction of the *mm* sequence and the ^{13}C spin–lattice relaxation time (T_{1C}) for the crystalline component of different stereoregular PVA samples.

crystallinity shown in Figs. 3 and 4, a clear minimum of the T_{1C} is also observed at an *mm* fraction of about 0.40. The *mm* fraction giving the T_{1C} minimum is somewhat lower than the corresponding fractions for T_m and crystallinity, probably suggesting that the T_{1C} may be affected not only by the crystallite size but also by the disordering extent of the structure. It should be, therefore, noted that the crystalline component might be more disordered in the sample with an *mm* fraction of about 0.40. In contrast, the T_{1C} value of the HI-PVA sample having the highest *mm* fraction is as high as about 260 s, which is much higher than that of A-PVA or S-PVA. This fact suggests that the crystalline chains of the HI-PVA may be much more rigid than those of S-PVA probably due to the successive formation of intramolecular hydrogen bonding since the crystallite size may be not significantly different from that of S-PVA.

As for the non-crystalline component, the T_{1C} value was found to be less than about 10 s for each sample regardless of the *mm* fraction. Since the ^{13}C magnetization observed by the CPT1 pulse sequence [41] exponentially decays with increasing relaxation delay time τ, a certain resonance line disappears by setting the τ to a value larger than 5 times of the T_{1C} of the line. Using this fact, the T_{1C}-filtered spectrum of the crystalline component was selectively measured for each sample by the CPT1 pulse sequence with $\tau = 40$–50 s in the same way as for A-PVA [20–22,24,25].

Fig. 11 shows the spectra of the crystalline components thus obtained for the PVA samples shown in Fig. 9. As already reported [20–25], the CH resonance line of the crystalline component of A-PVA splits into three lines designated as lines I, II, and III, which are assigned to the CH carbons that are, respectively, associated with two, one, and no intramolecular hydrogen bond(s) in the triad sequences with the all-*trans* conformation. Interestingly, the relative intensity of line I is markedly increased with increasing *mm* fraction and only line I is observed for HI-PVAs having the *mm* fractions higher than 0.70. The latter fact seems to imply that the crystalline component of HI-PVA may be composed of the *mm* sequences having intramolecular hydrogen bonded OH groups. However, the degrees of crystallinity are at least as high as 0.4–0.5 for these samples as shown in Fig. 4 and it must be, therefore, impossible to produce the crystalline chains composed of only the *m* units because of such a low *mm* fraction as 0.7.

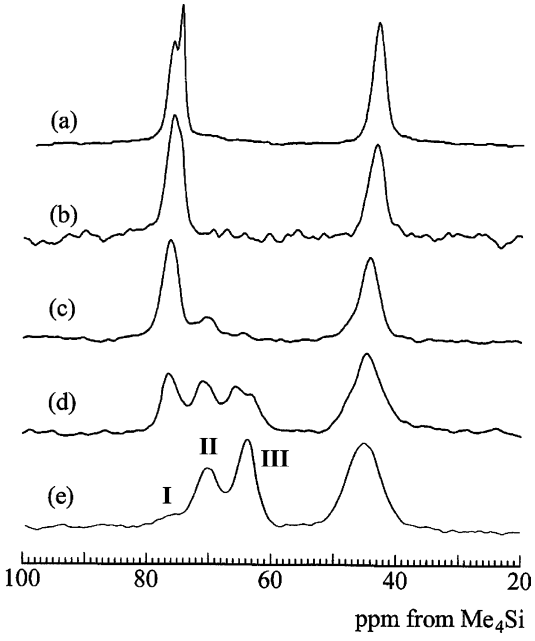

Fig. 11. CP/MAS ^{13}C NMR spectra of the crystalline component of different stereoregular PVA samples: (a) HI-PVA (*mm* = 0.79), (b) HI-PVA (*mm* = 0.70), (c) LI-PVA (*mm* = 0.59), (d) LI-PVA (*mm* = 0.50), (e) A-PVA.

Fig. 12 shows two model PVA sequences composed of the *mmrmm* unit: The one shown in Fig. 12(a) adopts the all-*trans* conformation and, therefore, intramolecular hydrogen bonding is not formed only in the *r* unit. In contrast, when the *gauche*$^+$ conformation is introduced to the CH–CH_2 bond in the *r* unit as shown in Fig. 12(b), the same type of intramolecular hydrogen bonding is allowed to form even in the *r* unit. This fact seems to support the preferential appearance of line I for the crystalline component of HI-PVA, although a prominent kink of the molecular chain axis is produced by the introduction of the *gauche* conformation as already pointed out [42]. Moreover, such a kink will be readily cancelled out by the introduction of the *gauche*$^-$ conformation as a pair at another position along the chain [42]. However, when some amounts of the *gauche* conformations are introduced, the so-called γ-*gauche* effect [43] should induce about 5 ppm upfield shift for the CH_2 and CH carbons compared to the case of the *trans* conformation. Since such upfield shifts are not actually observed for the CH and CH_2 resonance lines as seen in Fig. 11, normal types of *gauche* conformations should not be introduced in the crystalline region for HI-PVA although intramolecular hydrogen bonding must be really formed for all OH groups.

One possible way to overcome such difficulties is to set each torsion angle for each C–C bond to appropriate values that are not greatly deviated from the equilibrium value, 180°, at the *trans* conformation so as to allow to form intramolecular hydrogen bonding even in the *r* units. The distributions in the torsion angle may be reasonably narrow and each chain must adopt a slightly helical structure with a considerably long period. Since the CH line designated as line I splits into two

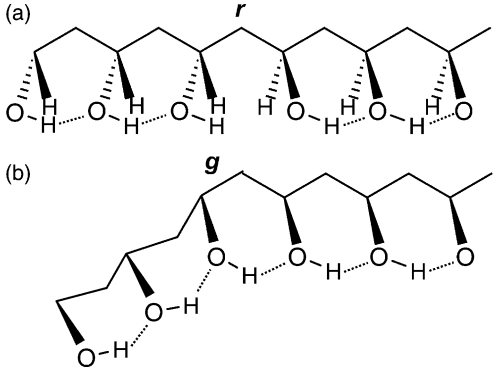

Fig. 12. Schematic representations of intramolecular hydrogen bonding forming for the *mmrmm* sequence with different conformations: (a) all-*trans* conformation, (b) disordered conformation containing *gauche* (*g*) in the *r* unit.

lines for HI-PVA as seen in Fig. 11, two types of the helical structures may be produced in the crystalline region probably depending on the probability of the *r* units appearing along each chain. Moreover, an appreciable upfield shift observed for line I with increasing *mm* fraction suggests the decrease in the strength of intramolecular hydrogen bonding, which may be induced by the increase in the O···O distance due to the deviation from the *trans* conformation. An actual helical structure will be explicitly created by computer simulations for a single PVA chain or an assembly of the chains particularly by considering the formation of intramolecular hydrogen bonding for each OH group in near future.

The integrated fractions of lines I, II and III for the crystalline component, which were obtained by the lineshape analysis [20–25], are plotted against the *mm* fraction in Fig. 13. Both of the integrated fractions of lines I and III are found to continuously change with the change of the *mm* fraction although their changes seem almost symmetric. In contrast, the fraction of line II has a maximum at the *mm* fraction of about 0.4, which well corresponds to the *mm* fractions giving the minima of T_m, degree of crystallinity, and T_{1C} shown in Figs. 3, 4, and 10, respectively. This fact suggests that the introduction of the *mr* units may induce significant disordering of the regular formation of intermolecular or intramolecular hydrogen bonding for the syndiotactic or isotactic sequences, respectively. However, in such a case, the maximum of line II would appear at the *mm* fraction of 0.25, which corresponds to the maximum *mr* fraction of 0.50. The cause of the deviation of the *mm* fraction giving the maximum of line II from 0.25 to about 0.4 may be due to the fact that the probability f_a of the formation of intramolecular hydrogen bonding in the *m* units will be less than 1.0. In fact, f_a was estimated 0.56 and 0.85 for the crystalline and non-crystalline components of A-PVA, respectively [25]. Moreover, the deviation will become larger since the f_a value must be decreased with decreasing *m* fraction. It should be, therefore, concluded that the basic properties of stereoregular PVAs are mainly dominated by the formation or disordering of intermolecular and intramolecular hydrogen bonding in the polymer chains.

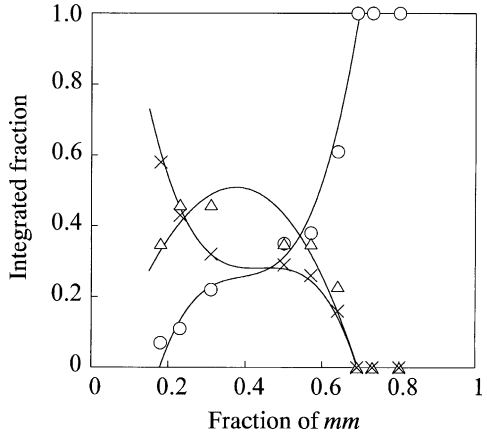

Fig. 13. Relationships between the *mm* fraction and the integrated fractions of line I (circle), II (triangle) and III (cross) for the crystalline components of stereoregular PVA samples.

4. Conclusions

We have characterized the structure, hydrogen bonding and some basic physical properties as a function of the *mm* fraction for different stereoregular PVA films including highly isotactic PVAs, which were successfully synthesized by evaluation of the polymerization recently, by using different analytical methods, and obtained the following conclusions:

(1) It has been confirmed that the triad tacticities are well interpreted in terms of the Bovey's statistical model in the wide range of tacticity. This fact suggests that the growing chain end and its penultimate unit may admit the statistically random addition reaction of the monomer irrespective of the difference in the polymerization methods used in this work.

(2) T_m, degree of crystallinity, and T_{1C} of the crystalline component have their own minima at the *mm* fraction of 0.4–0.5, implying that the decrease in crystallite size and the structural disordering may most significantly occur at this *mm* fraction.

(3) The appearance of a new crystalline band at about 1160 cm^{-1} in the FTIR spectra has reconfirmed the formation of a new type of crystal structure for isotacticity-rich PVA having the *mm* fractions higher than about 0.55, in good accord with the results previously obtained by wide-angle X-ray diffractometry. The relationship between the absorbance ratio, D_{916}/D_{849}, of the two bands and the syndiotacticity has been revised on the basis of the results of HI-PVA.

(4) The relative intensity for line I of the CH resonance line, which is assigned to the CH carbons associated with the formation of two intramolecular hydrogen bondings, is markedly increased with increasing *mm* fraction for the crystalline component and only line I is observed for HI-PVAs having the *mm* fractions higher than 0.70. This fact suggests that intramolecular hydrogen bonding is formed for all OH groups in the crystalline region for the HI-PVAs along the chains that contain some number of the *r* units and the respective chains may adopt a slightly helical structure with a considerably long period to allow the formation of such successive intramolecular hydrogen bonding.

(5) The lineshape analysis of the CH resonance lines of the crystalline components for the different stereoregular PVAs has revealed that the integrated fraction for line II, which is assigned to the CH carbons associated with one intramolecular hydrogen bonding in the *mm* or *mr* units, has a maximum at the *mm* fraction of about 0.4. Since this *mm* fraction well corresponds to the *mm* fraction giving the minima of T_m, degree of crystallinity and T_{1C}, it should be concluded that the disordering due to the introduction of irregular hydrogen bonding into successive intramolecular or intermolecular hydrogen bonding along each chain may induce the decreases in these physical values relating to the crystallinity.

References

[1] Fujii K. J Polym Sci, Part D 1971;5:431.
[2] Finch CA. Polyvinyl alcohol-developments. New York: Wiley; 1992 [chapters 9 and 10].
[3] Finch CA. Polyvinyl alcohol. New York: Wiley; 1973 [chapters 6 and 10].
[4] Murahasi S, Yuki H, Sano T, Yonemura U, Tadokoro T, Chatani Y. J Polym Sci 1962;62:S77.
[5] Yuki H, Hatada K, Oda K, Kinoshita H, Murahashi S, Ono K, et al. J Polym Sci, Part A-1 1969;7:1517.
[6] Okamura S, Kodama T, Higashimura T. Makromol Chem 1962;53:180.
[7] Higashimura T, Suzuki K, Okamura S. Makromol Chem 1965;86:259.
[8] Murahashi S, Nozakura S, Sumi M. J Polym Sci, Part B 1965;3:245.
[9] (a) Murahashi S, Nozakura S, Sumi M, Yuki H, Hatada K. J Polym Sci, Polym Lett Ed 1966;4:65.
(b) Murahashi S, Nozakura S, Sumi M, Yuki H, Hatada K. Kobunshi Kagaku 1966;23:550.
[10] Ohgi H, Sato T. Macromolecules 1993;26:559.
[11] Ohgi H, Sato T. Macromolecules 1999;8:2403.
[12] Ohgi H, Sato T. Polymer 2002;43:3829.
[13] Horii F, Hu S, Deguchi K, Sugisawa H, Ohgi H, Sato T. Macromolecules 1996;29:3330.
[14] Yamamoto T, Yoda S, Takase H, Sangen O, Fukae R, Kamachi M, et al. Polym J 1991;23:185.
[15] Finch CA. Polyvinyl alcohol-developments. New York: Wiley; 1992 p. 757.
[16] Nakajima A. Kobunshi Kagaku 1949;6:451.
[17] Moritani T, Kuruma I, Shibatani K, Fujiwara Y. Macromolecules 1972;5: 577.
[18] DeMember JR, Haas HC, MacDonald RL. J Polym Sci, Polym Lett Ed 1972;10:385.
[19] Horii F, Hirai A, Kitamaru R, Sakurada I. Cellulose Chem Technol 1985; 19:513.
[20] Horii F, Hu S, Ito T, Odani H, Kitamaru R, Matsuzawa S, et al. Polymer 1992;33:2299.
[21] Hu S, Horii F, Odani H, Narukawa H, Akiyama A, Kajitani K. Kobunshi Ronbunshu 1992;49:361.
[22] Hu S, Tsuji M, Horii F. Polymer 1994;35:2516.
[23] Masuda K, Horii F. Macromolecules 1998;31:5810.
[24] Masuda K, Kaji H, Horii F. Polym J 1999;31:105.
[25] Masuda K, Kaji H, Horii F. J Polym Sci, Part B: Polym Phys 2000;38: 1060.
[26] Ouchi M, Kamigaito M, Sawamoto M. J Polym Sci, Part A 2001;39:1060.
[27] Bovey FA, Tiers GVD. J Polym Sci 1960;44:173.
[28] Tubbs RK. J Polym Sci 1965;3:4181.
[29] Holland BJ, Hay JN. Polymer 2001;42:6775 [and references therein].
[30] Cooney TF, Wang L, Sharma SK, Gauldie RW, Montana AJ. J Polym Sci, Part B: Polym Phys 1994;32:1163.
[31] Murahashi S. Pure Appl Chem 1967;15:435 [and references therein].
[32] Sugiura K, Hashimoto M, Matsuzawa S, Yamaura K. J Appl Polym Sci 2001;82:1291 [and references therein].
[33] Fujii K, Fujiwara Y, Brownstein S. Prepr 17th Polym Symp (Matsuyama, Japan) 1968;1111.
[34] Tsuji H, Horii F, Nakagawa M, Ikada Y, Odani H, Kitamaru R. Macromolecules 1992;25:4114.
[35] Ishida H, Kaji H, Horii F. Macromolecules 1997;30:5799.
[36] Kuwabara K, Kaji H, Horii F, Bassett DC, Olley RH. Macromolecules 1997;30:7516.
[37] Kuwabara K, Kaji H, Horii F. Macromolecules 2000;33:4453.
[38] Ohira Y, Horii F, Nakaoki T. Macromolecules 2000;33:5566.
[39] Ohira Y, Horii F, Nakaoki T. Macromolecules 2001;34:1655.
[40] Murakami M, Ishida H, Miyazaki M, Kaji H, Horii F. Macromolecules 2003;36:4160.
[41] Torchia DA. J Magn Reson 1978;30:613.
[42] Assender HE, Windle AH. Polymer 1998;39:4303.
[43] Tonelli AE. NMR spectroscopy and polymer microstructure: the conformational connection. New York: VCH; 1989.